18TH WORLD CONFERENCE ON EARTHQUAKE ENGINEERING
WCEE2024
MILAN

MILAN, ITALY
30TH JUNE - 5TH JULY 2024
www.wcee2024.it

HARMONIZING SEISMIC PERFORMANCE VIA RISK TARGETED SPECTRA: STATE OF THE ART, DEPENDENCIES, AND IMPLEMENTATION PROPOSALS

Andrea Spillatura[1], Dimitrios Vamvatsikos[2], Mohsen Kohrangi[1], Paolo Bazzurro[3]

[1]RED – Risk Engineering + Development, Pavia, Italy
[2]School of Civil Engineering, National Technical University of Athens, Greece
[3]University School for Advanced Studies IUSS Pavia, Italy

SUMMARY

***Abstract**: Structures are typically designed on the basis of ground motion spectral values associated to an "ultimate" limit state of reference, e.g., 10% in 50 years, which gives a measure of the hazard at the site of interest. However, this design approach does not guarantee that the risk will be uniform, even for buildings at sites that share the same design level, as measured, e.g., by the peak ground acceleration, mainly because of differences in hazard curve shape. Aiming to ensure a uniform collapse risk across different sites and buildings, Risk Targeted design maps were first introduced by ASCE7-10 to modify conventional design spectra by employing suitable adjustment factors. As there is more than one approach to define such factors, our objective is to test their effectiveness in matching a specific target risk or, at least, in harmonizing the risk of multiple buildings at different sites with respect to different limit states. To do so, we make use of simplified single-degree-of-freedom structures for several configurations of vibration period and ductility. Although risk matching is shown to be only theoretically possible and unachievable in practice, we claim that harmonization remains a viable and valuable target.*

1 Introduction

Current provisions of many seismic design codes, including the present version of EN1998-1:2004EN1998-1:2004 (2004), follow a paradigm of designing on the basis of an intensity measure (IM) associated with a constant seismic hazard level, e.g. PGA at a 475-year return period. Consequently, every structural performance level, e.g., Damage Limitation or Life Safety, is checked using intensities associated to this predefined hazard level. This design procedure, which includes partial safety factors that increase actions and decrease material resistances, is assumed to provide a sufficient safety margin against loss of life due to earthquakes for newly designed buildings. Nevertheless, the seismic risk related to any performance level or limit state is not explicitly determined. Code design, therefore, may result in non-uniform risk for buildings located at different sites within a region (or country) having identical values of design ground motion intensity.

Arguably, the most comprehensive approach to tackle this issue is to introduce risk at the output level of the response, rather than at the input level of (design) spectral acceleration, conforming to risk-based views of performance-based design. A more practical (and limited) approach, conceptually stemming from the seminal work on environmental contours of Winterstein et al. (1993), was proposed instead by Luco et al. (2007). Their idea was to modify the input design spectral acceleration to a 'risk-targeted' (RT) value that indirectly accounts for the effects of hazard and fragility. Then, only the design spectra need to change, rather than the process of design.

Specifically, Luco et al. (2007) proposed to modify the seismic design maps of the US code provisions (e.g. ASCE 7-10 ASCE7-10 (2013)) into 'risk targeted maps' by means of Spectrum Adjustment Factors (SAFs) to

target a uniform mean annual frequency (MAF) of collapse. These maps were originally derived for spectral acceleration (S_a) at two periods (0.2s and 1.0s) that are the primary inputs needed to build the so-called two-period ASCE-type design spectrum ASCE7-10 (2013). The adjustment factors result from a risk analysis involving the definition of a *generic* collapse fragility curve consistent with the definition of FEMA P-695 FEMA-P695 (2009) strength reduction (or response modification) R-factors. These R-factors are determined specifically to yield a 10% probability of failure given the Maximum Considered Earthquake, MCE, which is typically defined at an S_a intensity level with a MAF of 2% in 50yrs. Keeping constant its assumed variability, the generic fragility curve is shifted, by means of adjusting the S_a at 10% collapse probability via an iterative procedure, until it produces the target MAF of collapse, originally taken as 1% in 50yrs; the ratio between the "shifted" S_a and the original one defines the SAF for the given period. The end result is that a structure designed to resist the seismic loads implied by the SAF-adjusted spectra, or RT spectra, will have a risk of collapse equal or lower than the targeted 1% in 50yrs, assuming of course that the structure performs precisely as the generic fragility says. This idea has been further tested and developed by several researchers (Douglas et al. (2013), Silva et al. (2016), Taherian and Kalantari (2019), Zarrineghbalb and Rahimianb (2021), Gkimprixis et al. (2019), Stewart J.P. et al. (2020), Heresi and Miranda (2023)) to produce risk targeted maps.

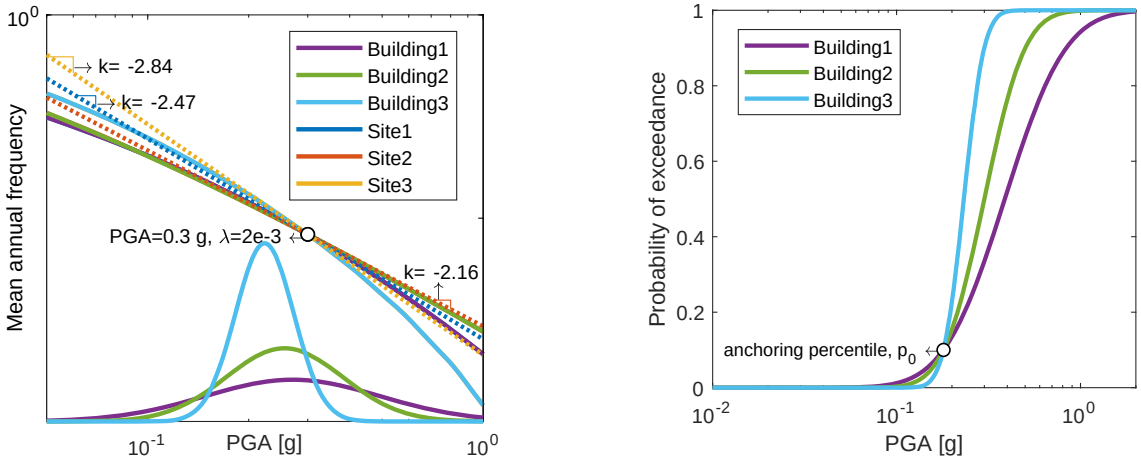

Figure 1 – (a) Hazard curves for three sites having the same design PGA at 10% in 50 years but different slope k (represented by the dashed tangent lines), and (b) three different fragility curves to be employed for risk harmonization, each representing a different weighting of the importance of the shape/slope of the hazard curve, all anchored at a percentile of $p_0 = 0.10$. The fragility curves, shown as cumulative distribution functions on the right, also appear in the form of probability density functions on the left, to better show the weighting at each PGA level (adopted from Spillatura et al. (2023))

All such versions of RT spectra represent different compromises between simplicity and accuracy. By virtue of defining a single design spectrum at each site, one effectively bundles together all types of structures (steel, masonry, etc.) that happen to have similar modal periods, using a 'structure-agnostic' generic fragility function to describe their behavior. Which and how many generic fragilities are used, what performance objective is targeted, and how the design spectrum is fitted are among the choices faced when applying RT spectra, each with its own pros and cons vis-à-vis ease of application and accuracy, all producing potentially different outputs and designs. To level the field, we shall discuss in detail the definition of each element of RT spectra applications and investigate its effect using simple single-degree-of-freedom (SDoF) systems to represent different buildings.

2 Elements of Risk-Targeted Spectra

Essentially, most if not all proposals for RT spectra can trace their origins to the Luco et al. (2007) approach. Its application on a site of interest and for a given period T can be broken down to the following steps:

- Define a generic fragility to represent “all” buildings of interest with period T; the fragility is characterized by a 10% probability of collapse (per FEMA P-695 FEMA-P695 (2009) calibration for USA) at the design ground motion S_a value at period T.
- Define a risk (or MAF) target, λ_{tgt}, i.e. 1% probability of collapse in 50 years.
- Define the site hazard curve for the IM of interest (e.g., $S_a(T)$).
- Integrate hazard with fragility to estimate the collapse MAF.
- Iteratively adjust the fragility curve, multiplying its median (or 10% value) by a factor of SAF, until the collapse MAF converges to λ_{tgt}, thus obtaining the optimal SAF.
- Multiply the original design spectra value at period T by the optimal SAF to obtain the corresponding RT spectra value.

This approach implies that designing a structure by the site RT spectra will ensure meeting the targeted collapse risk, as long as the resulting structure conforms to the generic fragility assumption. This process can be further generalized by breaking it down to its four fundamental elements (and associated user choices):

1. Fragility functions that describe the performance of the building stock. For a simple representation of the building stock, one employs a generic, structure-agnostic fragility curve definition for all building types and all sites within the region of interest, modifying it by shifting its central value, $IM_{c50\%}$, to reflect the difference in design intensities from site to site [1, 11, 12]. Such a generic fragility curve is essentially a mechanism for weighting the effect of the hazard curve shape (or its local slope) when estimating the risk that is targeted by the procedure. The anchor p_0 and MAF values determine the central point, $IM_{c50\%}$, of the fragility curve and, essentially, identify what part of the hazard curve one wants to emphasize in the risk computation. The dispersion, β, selects how broad or narrow the area of the hazard curve accounted for in the risk calculations will be.
2. Performance objective or, in other words, a limit state (LS), such as global collapse or life safety, coupled with a target MAF of exceedance, λ_{tgt}. The original proposals for RTGMs were mainly devised for the design of new structures by focusing on the collapse limit state. Nevertheless, current codes include also provisions to limit damage to structures for relatively low ground motion intensities. The choice of the LS to be targeted influences the anchoring percentile, p_0, that should be picked on the fragility curve corresponding to the selected LS.
3. Design spectrum shape and parametrization, namely the degree to which one can alter the shape of the spectra by optimizing ordinates at different periods to match the risk targets set. Seismic design codes typically provide a design spectrum whose intensity is defined by anchoring it to one or two spectral ordinates extracted from hazard maps. For simplicity we shall categorize the different design spectra based on the number of spectral ordinates that are employed to parameterize its shape.
    a. A flexible shape is the ideal case where any spectral ordinate can be individually adjusted for a particular site, akin to the multi-period spectra of ASCE 7-22.
    b. A semi-flexible shape, as originally adopted in ASCE 7-10 or in the forthcoming prEN1998-1-1:2022, is characterized by two anchor points, e.g., $S_{ds} = S_a(0.2s)$, and $S_{d1} = S_a(1.0s)$ in the former case.
    c. The rigid shape of a current EN1998-1:2004 spectrum is defined by a single pivot point, the PGA.
4. Spectral ordinates to be optimized, i.e. the range of periods and associated spectral ordinates that have been employed to tune the spectrum, and especially how these ordinates are weighted when considering a less-than-flexible spectrum shape.

3 Case study buildings and sites

The main goal is to investigate the effectiveness of the RT spectra approach in yielding uniform risk when designing new buildings and to quantify the effect of each of the aforementioned factors that play a role in its definition. In particular, as reference we use a set of sites located in six European cities characterized by the same design PGA, assuming that all the archetype structures analyzed in this study are founded on bedrock. To address the impact of building-specific fragility curves on the RT design procedure, we generated them for three different LSs and for multiple buildings with different ductility class and natural period, using

building- and site-specific fragility curves, rather than the generic fragilities similar to the approach of Luco et al. (2007) or Silva et al. (2016).

3.1 Selected sites and hazard computation

We chose two sets of three case study sites representing 'medium' and 'high' seismicity regions based on the web-based PSHA tool of EFEHR and the ESHM13 hazard model (Woessner et al. (2015). Three cities of Athens (Greece), Perugia (Italy) and Focșani (Romania) with coordinates of (37.976°N, 23.751°E), (43.111°N, 12.389°E) and (45.969°N, 27. 179°E) represent the high seismicity sites with PGA value on bedrock of about 0.30g for a 475-year return period (i.e. a_g=0.30g). The three cities of Baden (Germany), Montreux (Switzerland) and Aachen (Germany) with coordinates of (47.999°N, 16.218°E), (46.433°N, 6.899°E) and (50.776°N, 6.085°E) represent the medium seismicity sites with PGA value on bedrock of about 0.15g for a 475-year return period (i.e. a_g=0.15g). Figure 2a shows the location of the selected sites on the map and Figure 2b shows the corresponding hazard curves for PGA.

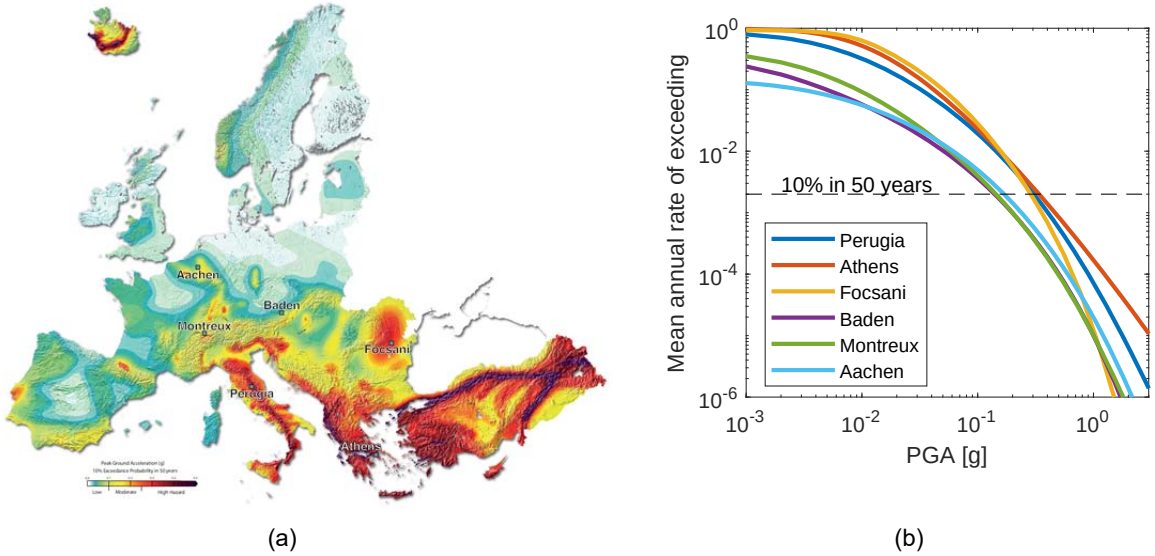

(a) (b)

Figure 2 – (a) Map of cities chosen as representative of high (red) and medium (blue) hazard sites, and (b) the corresponding PGA hazard curves. Adopted from Spillatura et al. (2023)

3.2 Structural systems, design procedure and limit state definition

Herein, SDoF systems are used as reference to model multiple buildings and structural systems. Clearly, using SDoF systems is a simplification and, therefore, it comes at a price: not considering the effects of higher modes, the influence of design minima or, more generally, all such matters that distinguish a real-world building from an SDoF proxy. However, we may expect to see similar trends. In addition, SDoFs allow us to investigate many more cases (i.e., archetype structures) and to perform a considerable number of dynamic analyses while updating the system characteristics according to the design requirements. To cover a wide range of different structures, our generic SDoF is defined with a bilinear elastic-hardening backbone, having a post-yield stiffness ratio of 3% and a kinematic hysteresis with no cyclic degradation. It is designed for two ductility levels, medium (ductility class medium, DCM) and high (ductility class high, DCH), and for fundamental periods of 0.5s, 1.0s and 2.0s. What we mean by "design" is the definition of the backbone characteristics of the SDoF: the ultimate displacement δ_u, the base shear coefficient C_y, and the yield displacement δ_y:

$$C_y = Sa_{UHS} \cdot \frac{OS}{q} \qquad \delta_y = C_y \cdot \frac{9.81}{(2\pi/T_1)^2} \qquad \delta_u = \mu_u \cdot \delta_y \tag{1}$$

T_1 is the fundamental period of the structure; μ_u is the ultimate ductility; Sa_{UHS} is the spectral acceleration at T_1 obtained from the uniform hazard spectrum of the site; q and OS are, respectively, the behavior factor and the over-strength, here taken to be dependent on the ductility class of the system; C_y is the base shear coefficient, which is equal to the maximum base shear strength divided by the total weight, numerically equivalent to the yield spectral acceleration in units of g.

Table 1 – Behavior factor and overstrength assumptions

Ductility class	Behavior factor q	Overstrength OS	Ultimate ductility μ_u
DCH	$q = 4.5 \cdot a_u/a_1 = 4.5 \cdot 1.3 = 5.85$	2.0	7
DCM	$q = 3.0 \cdot a_u/a_1 = 3.0 \cdot 1.3 = 3.90$	1.5	5

Table 2 – Limit state definitions in terms of the median ductility capacity and its dispersion, assuming lognormality

Limit State	DCH		DCM	
	Median, $\hat{\mu}$	Additional dispersion, β_U	Median, $\hat{\mu}$	Additional dispersion, β_U
Global Collapse (LS3)	7.0	0.3	5.0	0.3
Severe Damage (LS2)	3.5	0.3	2.5	0.3
Moderate Damage (LS1)	1.5	0.2	1.5	0.2

To maintain a certain level of realism, the behavior factor is taken according to EN1998-1:2004 provisions for reinforced concrete moment resisting frames as a function of the ductility class (Table 1) and of the a_u/a_1 ratio of ultimate base shear over the base shear at first yield. In order to include the uncertainty in LS definition, we incorporated via a square-root-sum-of-squares rule an additional dispersion of β_u = 0.2 – 0.3, with larger values employed for the more uncertain LSs (Table 2).

4 Fragility curves and Preliminary Assessment: How well can we harmonize?

Two conceptually different kinds of fragility curves can be considered. The first is represented by building-and-site specific fragility curves obtained by means of a PSHA-based record selection applied to the generic SDoF systems representing a wide variety of structures. The second kind is defined in line with the currently preferred 'generic' fragility approach, disregarding any site or building dependence beyond the fundamental period and the design intensity at the site of interest. Solely the first kind of fragility curves will be presented herein while results and analyses related to the generic functions can be found in Spillatura et al. (2023).

The fragilities to be employed are derived specifically for each site and SDoF system (building) described in the previous section. To do so, for each case-study, a 'single-site' set of 30 records has been selected by means of the Conditional Spectrum (CS) approach Baker (2011) based on the IM chosen to describe the severity of ground shaking. The record selection has been performed on the basis of the PSHA disaggregation data of the site, as estimated at the EN1998-1:2004 design hazard level of 10% probability of exceedance in 50 years. For the sake of simplicity and conciseness we will show the results solely related to the "usual" IM of spectral acceleration at the first modal period of the structure, $S_a(T_1)$, Baker (2011), Lin et al. (2013). The result is a total of (3 SDoFs × 6 sites) 18 site-and-building specific record sets. Note that the same sets of records are used for all DCH and DCM SDoFs with the same fundamental vibration period.

Incremental dynamic analysis (IDA) (Vamvatsikos and Cornell (2002)) is applied for all the defined cases, assuming that the same set of records is appropriate for application at all levels of intensity. This hypothesis may introduce a certain level of (usually conservative) bias to our final output. Nevertheless, following the recommendations of Kohrangi et al. (2020), we accept this additional uncertainty to reduce our computational burden. Figure 3 shows the results for a DCH 1.0s structure located in Athens. Figure 3a

shows the 16/50/84% IDAs in terms of ductility versus strength ratio, i.e. the $S_a(T_1)$ value divided by its value at yield. The corresponding (lognormally fitted) fragility curves appear in Figure 3b.

After the definition of the fragility and the cointegration with the hazard curve, we have the initial, un-harmonized case of Figure 4, showing the MAF distribution according to the different combinations of ductility class, period, city, and LS. This effectively represents the implicit risk of the SDoFs when designed according to EN1998-1:2004. The results are shown using a boxplot representation: the edges of the colored boxes depict the first and the third quartiles, Q_1 and Q_3 (o 25% and 75% percentiles), while the mid-point (shown as a black dot) depicts the median; circles appearing outside of each box are “outliers”, away from Q_1 and Q_3 by more than 1.5 times the interquartile range of Q_3-Q_1. Overall, when grouping all sites together, the median of the MAF values seems to be relatively constant with period for any given LS (Figure 3b). Still, the MAF variability per individual structure is quite substantial, as highlighted by the size of the boxes. The obvious question is whether there is a trend, or systematic bias, to this variation. Figure 5 shows the same data as in Figure 4 only reshaped in order to appreciate the effect of the site for each of the cities considered in this study. As expected, now there are evident differences in the achieved performance from site to site for all LSs. Note here a minor departure from what has been observed in recent literature, and especially in the RINTC project Iervolino I. et al. (2018, RINTC-Workgroup (2018). Due to the enforcement of code minima (see, for example, Žižmond and Dolšek (2016)) and associated capacity design rules, buildings designed according to high-ductility rules at moderate/low-seismicity sites will, in general, have higher overstrength than similar configurations designed in high-seismicity areas. This would mean lower MAFs (i.e., higher performance) of exceeding different LS in buildings designed for lower hazard sites compared to buildings at higher hazard sites. Due to the site-independent overstrength values adopted in Table 1, this trend is not observed when comparing Figure 5a to Figure 5b. Appropriately incorporating such a disparity with a faithful definition of fragility curves can become a powerful argument in favor of building/site-specific versus generic fragility curves. Still, for the purposes of our investigation this is not considered any further.

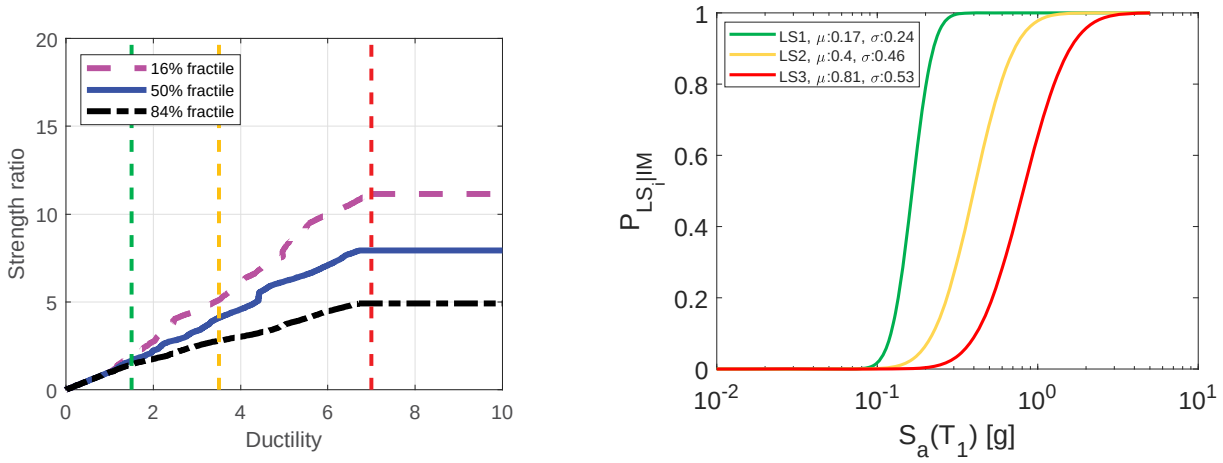

(a) (b)

Figure 3 –DCH structure with T_1=1.0s designed for Athens: (a) percentile normalized IDA curves for $S_a(T_1)$ and (b) corresponding LS fragility curves represented by their median μ and logarithmic standard deviation σ. The vertical dashed lines represent the (median) displacement threshold used to define the onset of LS1 (green), LS2 (orange) and LS3 or collapse (red). Adopted from Spillatura et al. (2023)

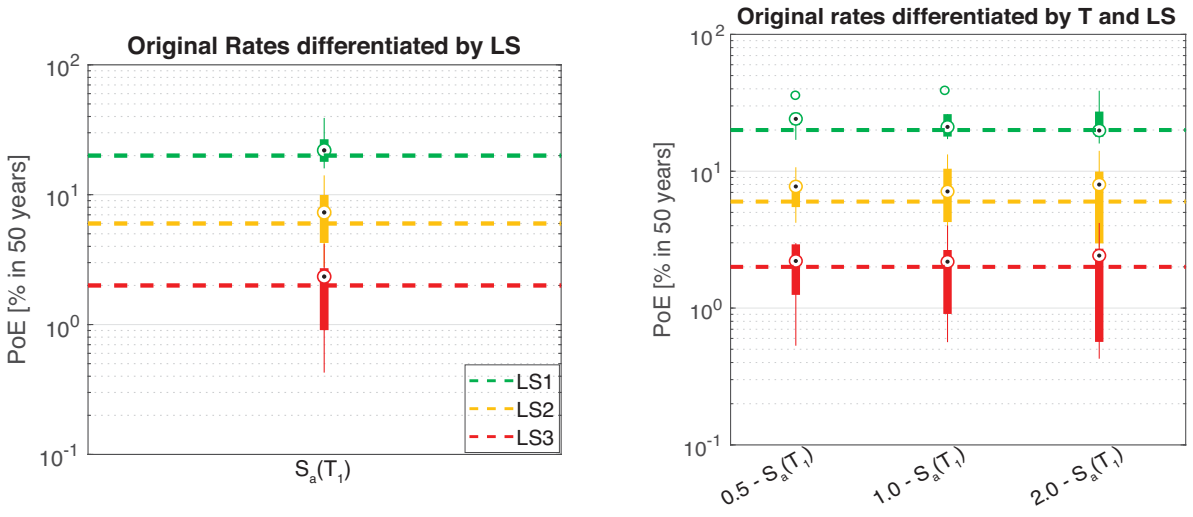

(a) (b)

Figure 4 – Initial MAF distribution for LS1 (green), LS2 (yellow) and LS3 (red) for SDoFs with different periods computed using $S_a(T_1)$. Results from all sites are grouped together, differentiating only by (a) LS and IM type versus (b) period, LS and IM type. The horizontal dashed lines indicate proposed LS harmonization target MAFs that are close to the resulting initial median MAFs. Adapted from Spillatura et al. (2023)

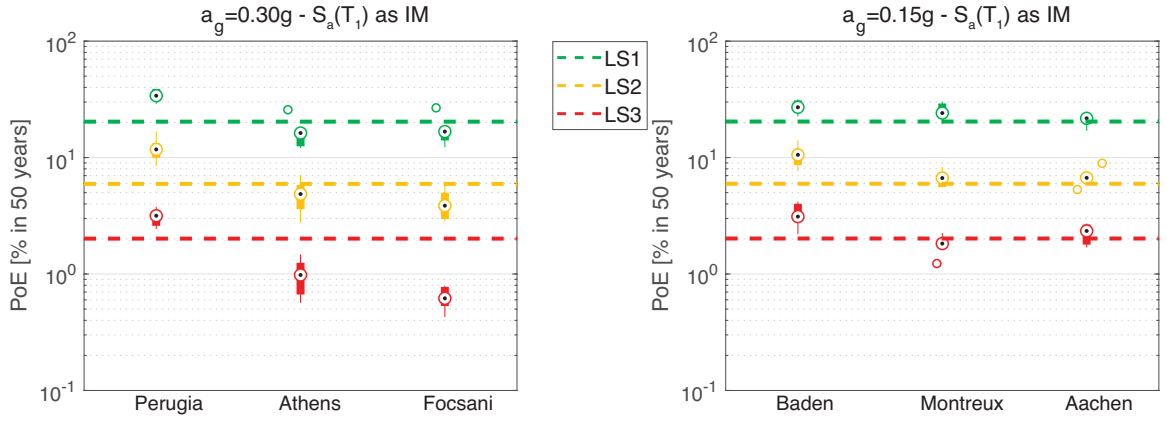

(a) (b)

Figure 5 – Initial MAF distribution for LS1 (green), LS2 (yellow) and LS3 (red) differentiated by cities belonging to (a) high and (b) moderate hazard zones. Adopted from Spillatura et al. (2023)

5 Risk targeted Spectra: calculation and practical impact

Given a performance objective, estimation of the SAF is a straightforward process of adjusting the design intensity of Sa_{UHS}, estimating the new corresponding fragility curve, estimating the new limit-state MAF and repeating until convergence (see Section 2). It is only the estimation of the fragility that may need some further elaboration: for the generic fragility curves, this process is trivial, as one directly scales the central value of the fragility via the adjusted design IM level that corresponds to the anchor probability of p_0. Given the lognormal shape of the fragilities, this means that the adjusted median fragility capacity in terms of S_a becomes:

$$Sa_{c50\%} = Sa_{UHS} \cdot SAF \cdot exp(K_{p0} \cdot \beta) \quad (2)$$

K_{p0} is the standard normal variate that corresponds to p_0, i.e., $K_{p0} = \Phi^{-1}(p_0)$, where $\Phi(\cdot)$ is the standard normal cumulative distribution function. For SDoF-based building-specific fragility functions, estimating the fragility is only slightly more complex as it actually requires "redesigning" each SDoF system. Practically speaking the system properties need to be modified according to Equation (3) to match the new design intensity. Thus, the strength of the system becomes:

$$C_y = S_{a,UHS} \cdot SAF \cdot \frac{OS}{q} \tag{3}$$

By virtue of having the IDA results in terms of R and μ for a given system, we can painlessly derive the IDA curves for different yield base shear values (of the otherwise same system) by denormalizing to the new yield values. This means that finding the fragility median, $IM_{c50\%,}$ for any base shear value becomes only an issue of postprocessing. After all, since our limit-states are based on ductility thresholds, the fragility dispersion remains unchanged.

We are going to employ a single target MAF for each LS targeted across all building and site combinations. To avoid large values of SAFs, i.e., major adjustments in the design spectrum, we shall set as provisional target an approximate value near the median of the MAF values that have been observed per LS, namely 20%, 6% and 2% in 50 years for LS1, LS2 and LS3, respectively (see Figure 4). Once the SAFs are computed, it is interesting to evaluate their actual impact on the resulting MAFs based on the method of estimation/application, and whether their adoption can indeed provide some universal advantages, particularly for non-targeted cases, e.g. the structures or LSs for which the SAFs are not optimized.

Note that the actual implementation of the SAF factor is highly dependent on the design spectrum shape and on its flexibility in capturing the different SAFs required at each period. Even for our limited case study of three different periods, the harmonization procedure results in three different SAFs, i.e. three spectral acceleration ordinates to which the code spectrum could be fitted. In the Semi-Flexible approach case, we shall employ the T=0.5s SAF to directly determine the plateau, while the constant velocity 1/T segment will be determined from the T=1s and 2s values by minimizing the sum of squared errors. This may not necessarily produce an ASCE 7-10 compatible spectrum, especially if the corner period, where the constant acceleration plateau and the constant velocity segment intersect, ends up being shorter than 0.5s. Still, this did not become an issue in our investigation. In the case of a Rigid EN1998-1:2004 style spectrum, all three SAFs can be used separately to scale up the spectrum or employed together to obtain an optimal fit. In the latter case, the anchoring spectral ordinate (PGA) of the spectrum is simply estimated by minimizing the sum of the squares of the errors for the three spectral coordinates.

6 Results

To quantify the effect of applying different combinations of target limit-states and spectrum shapes, we compute the variability in terms of the coefficient of variation (COV) of the MAFs and we also offer the average normalized bias with respect to the targeted MAF; both are estimated over sets of different sites and buildings. The bias is meant to measure accuracy, i.e., how well each approach captures the target MAF. A low error signifies a method that can “guarantee” the target MAF at least for a single LS definition. On the other hand, the COV also conveys the degree of harmonization, i.e., the uniformity of the MAF values among the different systems, sites, periods, and LS definitions, regardless of whether the target MAF is met.

Figure 6 depicts the impact of employing building-specific fragility curves with a Flexible shape spectrum compared to the other spectrum shapes (i.e., Rigid and Semi-Flexible). In this exercise for estimating SAFs we targeted only the SDoFs in the DCH subset and only one of the three LSs at the time and we employed S_a as the response predictor IM. It can be said that after whatever kind of harmonization we employ in terms of IM, system subset or spectrum shape, we do observe significant decrease of the variability of the MAF. Given the adopted strategy that targets one LS for one SDoF, the best result (i.e., a “perfect” match of the target MAF) is obviously achieved for the individual SDoF systems for which the SAFs are computed. The bar related to the targeted SDoF and LS, in fact, disappears from the charts in the left column of Figure 6. This way of proceeding, however, is impractical beyond the confines of our study. Customizing SAFs to a particular structure cannot be employed in code-level RT spectra applications. At the same time, considering a web-tool that offers some customization of RT-spectra for the salient characteristics, e.g., period, ultimate ductility, overstrength, of any system of interest could be a valuable proposition to pursue, especially if the variation in resulting design values is significant relative to all the other uncertainties in the design process. If “perfect” matching of the target MAF is sought, this would arguably be the best approach for implementing RT-spectra at a code level.

As the MAF variabilities in Figure 6 clearly show, this approach is not very effective in achieving a match of the target MAF even using all DCH buildings (i.e., one half of the building population) to derive the SAFs:

neither for different LSs on the same DCH structures, nor for any other LSs (even the specific LS targeted by the procedure) for the DCM structures. Any deviation from the set employed for optimization produces bias. However, there is a consistent reduction of about 50% in COV values of the MAF of every LS with respect to the corresponding initial values (Figure 4), i.e. the MAF values without RT-spectra application. The procedure does not necessarily provide the MAF that we are targeting, but it guarantees less variability among the MAFs of every LS for buildings of different designs. In other words, RT-spectra computed for a single LS seem to harmonize the MAF across different buildings, sites, and LSs, probably as a side-effect of taking care of the hazard curve shape/slope influence; yet they cannot make the MAF of any LS match a specific target, even for basic SDoF systems.

Looking across different LSs, the single LS employed to derive the SAFs (for example, LS3 for the bottom row of Figure 6) will get the highest level of harmonization, or lower overall COVs. As already mentioned, the effect spreads to a certain degree also to the other non-targeted LSs. The LS further from the target, namely LS1 if the harmonization is performed for LS3 (Figure 6, bottom panel on the right), does receive the lower benefits (i.e., a relatively higher COV) but still better than having no harmonization at all. A good compromise is reached when the harmonization is performed for LS2, yielding relatively similar and low COVs for both LS1 and LS3. Given that monetary loss, rather than collapse, is cited as the main (and more frequent) consequence of seismic events for newly designed buildings (Ramirez (2013)), achieving harmonization across multiple limit-states can be widely beneficial in capturing the performance of the building stock where it matters the most. Therefore, in our opinion LS2 is a useful target for RT design spectra.

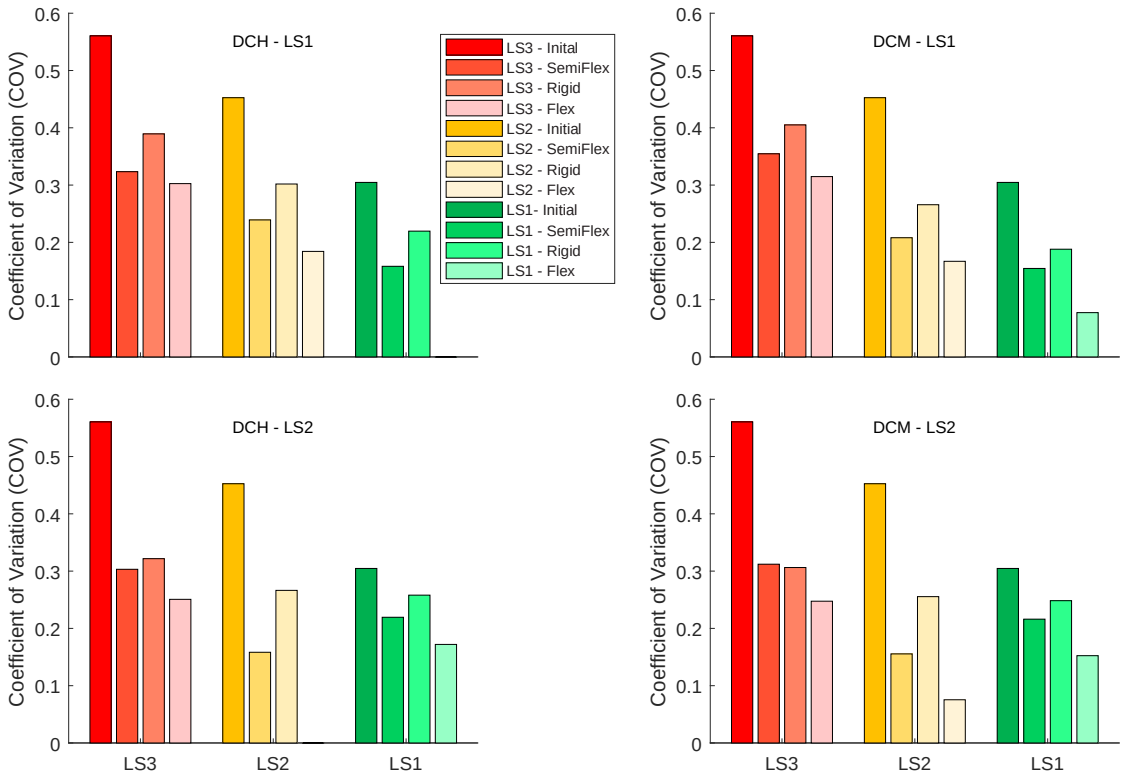

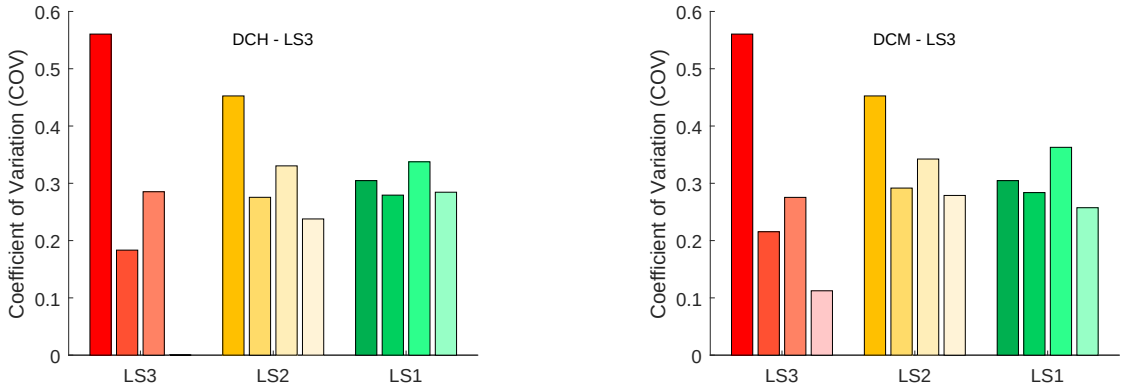

Figure 6 – Building-specific fragilities with various spectrum-shapes. COV of the MAF of the specific LSs of DCH (left) and DCM (right) structures. Each row represents a different target LS. SAFs are estimated only for the DCH structure subset at each period. The targeted case (DCH-LS$_i$) has always zero COV. Adopted from Spillatura et al. (2023)

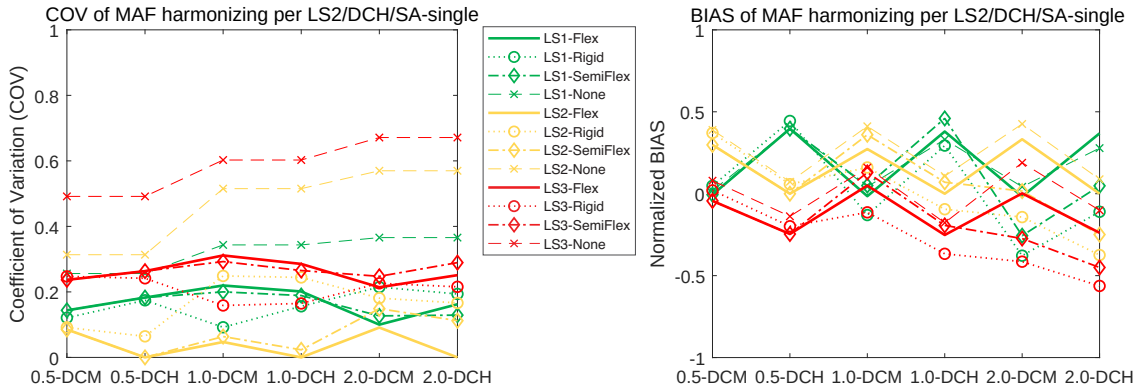

Figure 7 – The effect on estimated MAFs for building-specific fragilities with different RT spectra shapes (Rigid/Semi-Flexible/Flexible) versus initial spectra ("Initial"). COV (left) and BIAS (right) using S_a as IM and targeting LS2. SAFs are estimated only for the DCH subset at each period. Adopted from Spillatura et al. (2023)

Additional, perhaps more subtle, advantages can also be gained by targeting an intermediate limit-state like LS2, when considering EN1998 applications. The reason is the disparity between the targeted limit-state MAF, λ_{tgt}, and the fragility anchor intensity MAF of λ_0. If the two MAFs are widely different, then the anchoring percentile, p_0, will have to make up for the difference, moving further into the lower tail of the fragility. Employing low MAF hazard estimates together with the far-left tail of the distribution of the collapse capacity, where our lognormality assumption places non-zero collapse probability even for extremely low IMs, is not a recipe for robust results. Even if our data were somehow perfect, this would not make sense from an optimization standpoint, as we would not be harmonizing for the body of our building stock, but for the few bad buildings that might fail during an extreme phenomenon. Instead, targeting an LS2-like limit-state for EN1998, allows us to pull back to more reasonable p_0 values in the order of 0.10 – 0.20, which can be estimated with more confidence. The results clearly show that the benefits spread to LS3 anyway, so collapse probabilities are not left unattended.

Spectrum flexibility obviously has an impact as well. A Flexible shape generally offers good harmonization typically on par with the Semi-Flexible case but with some random exceptions for off-target cases. In further support of this observation, Figure 7 shows the results solely for the LS2 normalization case using the subset of DCH buildings, differentiating for ductility class and period of the structure. Therein, the impact of spectrum flexibility becomes clearer; indeed the Semi-Flexible case is more or less coincident with the Flexible case at a period of T=0.5sec; this is to be expected as this spectral ordinate fully defines the constant acceleration plateau in the Semi-Flexible case, allowing it to perfectly match the optimal SAF, similarly to the Flexible case. When moving to T=1sec or T=2sec where the Semi-Flexible shape can only

use one parameter (or SAF) to match two MAFs, the flexible approach is clearly better. Still, the most important conclusion remains that, regardless of the risk targeting approach adopted, the improvement with respect to the initial case is evident.

7 Concluding remarks

Risk-targeted (RT) spectra can be computed in a myriad of combinations, targeting different limit-states and corresponding MAFs, employing building-specific fragilities and optimizing different period ranges to adjust design spectra shapes of differing parameterization and flexibility. In all cases tested, one single theme seems to emerge: RT-spectra are not a panacea. They simply cannot guarantee risk *matching* for any limit-state across buildings and sites. On the other hand, they are fairly effective risk *harmonization* tools. A given risk level may not be matched for any specific building, but similar risk values are achieved across different buildings and sites. And this is not a negligible result.

Overall, RT spectra do confer considerable benefits practically regardless of the method used to determine them. Therefore, unless one goes all the way to implement building-specific fragilities, it makes little sense to overcomplicate their mode of application. Based on our limited investigation, there are some simple pointers to follow that generally make for better single- or multi-LS risk harmonization: (i) avoiding large disparities between the target MAF and the fragility anchoring intensity MAF of the code design spectrum; (ii) targeting an intermediate LS to better harmonize for frequent structural and non-structural damage; (iii) having more flexibility in the design spectrum shape to allow better harmonization at multiple periods; (iv) thinking of the target MAF as a point around which harmonization occurs, rather than an actual target to match.

8 Acknowledgements

Financial support has been provided by the Hellenic Foundation for Research and Innovation (H.F.R.I.) under the “2nd Call for H.F.R.I. Research Projects to support Faculty Members & Researchers”, Project “TwinCity: Climate-Aware Risk and Resilience Assessment of Urban Areas under Multiple Environmental Stressors via MultiTiered Digital City Twinning” (Grant Agreement 2515) and by the European Framework Programme for Research and Innovation (Horizon 2020) under the “YADES” Marie Skłodowska-Curie project with Grant Agreement No 872931.

9 References

ASCE7-10 (2013). Minimum Design Loads for Buildings and Other Structures. Reston, VA., American Society of Civil Engineers.

Baker, J. W. (2011). "The conditional mean spectrum: A tool for ground motion selection." ASCE Journal of Structural Engineering **137**: 322–331.

Douglas, J., T. Ulrich and C. Negulescu (2013). "Risk-targeted seismic design maps for mainland France." Natural Hazards **65**(3): 1999-2013.

EFEHR. "Share online tool for Hazard and UHS calculation." from http://www.efehr.org:8080/jetspeed/portal/browsers.psml.

EN1998-1:2004 (2004). Design of Structures for Earthquake Resistance - Part 1: General rules, seismic actions and rules for buildings. Brussels, Belgium.

FEMA-P695 (2009). Quantification of Building Seismic Performance Factors. 201 Redwood Shores Parkway, Suite 240, Redwood City, California 94065 Applied Technology Council for the Federal Emergency Management Agency.

Gkimprixis, A., E. Tubaldi and J. Douglas (2019). "Comparison of methods to develop risk-targeted seismic design maps." Bulletin of Earthquake Engineering **17**: 3727–3752.

Heresi, P. and E. Miranda (2023). "Regional-risk-targeted seismic design: A novel approach for earthquake resistant design." Earthquake Engineering & Structural Dynamics **52**(13): 3983-4008.

Iervolino I., Spillatura A. and Bazzurro P. (2018). "Seismic Reliability of Code-Conforming Italian Buildings." Journal of Earthquake Engineering **22**: 5-27.

Kohrangi, M., D. Vamvatsikos and P. Bazzurro (2020). "Multi-level conditional spectrum-based record selection for IDA." Earthquake Spectra **36**(4): 1976-1994.

Lin, T., S. C. Harmsen, J. W. Baker and N. Luco (2013). "Conditional spectrum computation incorporating multiple causal earthquakes and ground motion prediction models." BSSA **103**(2A): 1103–1116.

Luco, N., B. R. Ellingwood, R. O. Hamburger, J. D. Hooper, J. K. Kimballm and C. A. Kirchner (2007). Risk-targeted versus current seismic design maps for the conterminous United States. SEAOC convention proceedings.

Ramirez, C. M. a. M., E. (2013). Building-Specific Loss Estimation Methods & Tools for Simplified Performance-Based Earthquake Engineering, John A. Blume Earthquake Engineering Center, Technical Report 171.

RINTC-Workgroup (2018). Results of the 2015-2017 implicit seismic risk of code-conforming structures in Italy (RINTC) project. Naples, Italy, Rete dei Laboratori Universitari di Ingegneria Sismica (ReLUIS).

Silva, V., H. Crowley and P. Bazzurro (2016). "Exploring Risk-Targeted Hazard Maps for Europe." Earthquake Spectra **32**(2): 1165-1186.

Spillatura, A., D. Vamvatsikos, M. Kohrangi and P. Bazzurro (2023). "Harmonizing Seismic Performance via Risk Targeted Spectra: State of the art, dependencies, and implementation proposals." Earthquake Engineering & Structural Dynamics **52**(13): 4277-4299.

Stewart J.P., Luco N., Hooper J.D. and C. C.B. (2020). "Risk-targeted alternatives to deterministic ground motion caps in U.S. seismic provisions." Earthquake Spectra **36**(2): 904-923.

Taherian, A. R. and A. Kalantari (2019). "Risk-targeted seismic design maps for Iran." Journal of Seismology **23**: 1299–1311.

Vamvatsikos, D. and C. A. Cornell (2002). "Incremental dynamic analysis." Earthquake Engng. Struct. Dyn. **31**(3): 491–514.

Winterstein, S. R., T. C. Ude, A. C. Cornell, P. Bjerager and S. Haver (1993). Environmental parameters for extreme response: Inverse FORM with omission factors. Proceedings of ICOSSAR-93. Innsbruck, Austria.

Woessner, J., D. Laurentiu, D. Giardini, H. Crowley, F. Cotton, G. Grünthal, G. Valensise, R. Arvidsson, R. Basili, M. B. Demircioglu, S. Hiemer, C. Meletti, R. W. Musson, A. N. Rovida, K. Sesetyan, M. Stucchi and S. C. The (2015). "The 2013 European Seismic Hazard Model: key components and results." Bulletin of Earthquake Engineering **13**(12): 3553-3596.

Zarrineghbalb, A. Z., Hamid and M. Rahimianb (2021). "Towards an Iranian national risk-targeted model for seismic hazard mapping." Soil Dynamics and Earthquake Engineering **141**.

Žižmond, J. and M. Dolšek (2016). "Evaluation of factors influencing the earthquake-resistant design of reinforced concrete frames according to Eurocode 8." Structure and Infrastructure Engineering **12**(10): 1323-1341.